N_2O decomposition catalysed by transition metal ions

Alexei L. Yakovlev [a], Georgy M. Zhidomirov [b] and Rutger A. van Santen [a]

[a] *Eindhoven University of Technology, PO Box 513, 5600 MB Eindhoven, The Netherlands*
E-mail: A.L.Yakovlev@tue.nl; R.A.v.Santen@tue.nl
[b] *Boreskov Institute of Catalysis, pr. Lavrentieva 5, 630090 Novosibirsk, Russia*
E-mail: zhi@catalysis.nsk.su

Received 23 November 2000; accepted 15 May 2001

The direct N_2O decomposition catalysed by 5-coordinated transition metal ions Fe, Co, and Rh was studied using the DFT method. The cluster model has the formula $M(OH)_3(H_2O)_2$. Energies of intermediates and transition states were computed. The results show that Co and Rh sites are more active than Fe, the former two being very similar.

KEY WORDS: N_2O decomposition; DFT calculations; iron; cobalt; rhodium; transition states

1. Introduction

Nitrous oxide pollution abatement is an important environmental problem due to the high greenhouse potential of N_2O and its ozone-depleting properties. One of the available options is the direct catalytic N_2O decomposition. Kapteijn *et al.* [1] presented an excellent review on catalytic N_2O decomposition. According to it, active catalysts often contain copper, cobalt, iron, or noble metals such as palladium, rhodium, ruthenium, *etc.* Different catalysts show different sensitivity to other gases such as water, NO_x, oxygen. For example, copper catalysts are strongly inhibited by oxygen but the iron-containing ones are not. NO poisons most catalysts, however it promotes the reaction catalysed by Fe-ZSM-5 since it removes the adsorbed oxygen to form NO_2. Generally all catalysts are poisoned by water to a different extent. Thus most catalysts active in the presence of water, NO_x and oxygen were found to contain iron, cobalt, rhodium, and ruthenium.

We consider the following catalytic cycle in this study:

$$X + N_2O \rightleftharpoons X{\cdot}N_2O \tag{1}$$

$$X{\cdot}N_2O \rightarrow XO + N_2 \tag{2}$$

$$XO + N_2O \rightleftharpoons XO{\cdot}ON_2 \tag{3}$$

$$XO{\cdot}ON_2 \rightarrow XO_2 + N_2 \tag{4}$$

$$XO_2 \rightleftharpoons X + O_2 \tag{5}$$

This is essentially the Eley–Rideal mechanism [2] in which steps (1) and (2), and (3)–(5) are grouped together. Here X denotes an initial state of the active site, in the case of transition metal catalysts it is a cation exposed to the surface. The first step (1) is the physical adsorption of nitrous oxide on the site. The step (2) is the dissociation of the adsorbed N_2O molecule yielding a gas-phase N_2 molecule and an active surface oxygen atom. The steps (3) and (4) are the physical adsorption and decomposition of the second N_2O molecule, respectively. The product of the fourth step is an adsorbed oxygen molecule. Finally, the fifth step is desorption of the oxygen molecule, which closes the catalytic cycle. Activation energies of each step depend on the catalysts under study but for most catalysts the following pattern is observed. The molecular adsorption steps (1) and (3) proceed without activation energy and the heat of adsorption is not too high. For most catalysts the reaction (2) has a lower activation energy than reactions (4) and (5), although this depends on the metal ion and its oxidation state. Usually both (4) and (5) have comparable rate constants but in some cases (*e.g.*, Fe-ZSM-5) the step (4) is rate limiting. An alternative mechanism includes the steps (1) and (2) and the recombination of surface oxygen atoms:

$$2XO \rightarrow 2X + O_2 \tag{6}$$

This is the Langmuir–Hinshelwood mechanism, which plays an important role for oxide surfaces at higher temperatures [3]. However, for some systems such as zeolite-supported transition metal catalysts or diluted mixed oxides, where active sites are isolated, the role of the latter mechanism is insignificant.

The aim of this study is to compare the activity of different metal ions, *i.e.*, iron, cobalt, and rhodium, in N_2O decomposition. With this in mind, we determined the reaction energy diagrams of the reaction catalysed by single sites, including energies of intermediates and activation energies, as well as the nature of the metal–oxygen bonds in adsorption complexes and the nature of the transition states. We also compare present results with those obtained for similar Al-containing models [4] and with available experimental data.

2. Computational details

The active site is modeled by a cluster with the formula $M(OH)_3(H_2O)_2$, where M = Fe, Co, Rh (see figure 1). The

1011-372X/01/0800-0045$19.50/0

Figure 1. The $M(OH)_3(H_2O)_2$ cluster used as a model of the active sites.

model is further referred to as X. This cluster model represents some of the surface species that can be observed on the metal oxide surface or in zeolite cavities. All metals discussed here have an oxidation state III as one of the commonly encountered. Although for Fe and Co the oxidation state II is often the initial one after the catalyst's preparation, under reaction conditions in the absence of reducing agents (such as hydrocarbons) the oxidation state III should be considered as a reference.

We used models like this earlier to study N_2O decomposition on Al-containing Lewis acid sites [4]. The geometry optimisation procedure was also adopted from [4]. All the obtained transition states were verified to have only one imaginary vibration frequency at the final geometry.

In our calculations we used the Amsterdam density functional (ADF) program [5] which employs DFT in combination with STO basis sets. For the present study, double-zeta basis sets with frozen core and the Perdew-Wang91 (PW91) gradient corrected exchange and correlation functionals [6] were used. The level of the present calculations is sufficient to draw qualitative conclusions about comparative catalytic activity of the related systems, such as those presented here. Iron-containing models were calculated with five unpaired electrons; this configuration corresponds to the state with the total spin 5/2. For cobalt and rhodium models spin-restricted calculations were performed.

3. Results and discussion

Main results of the calculations are summarized in table 1. The graphical representation of the energy diagrams for different metals of the reaction is shown in figure 2. Interestingly, the reaction profiles for Rh, Co are very similar to each other but they are quite different from that for Fe. Rh^{3+} and Co^{3+} appear to be more reactive catalysts than Fe^{3+}. The most important parameters determining the reaction rate are the heights of the reaction barriers (transition state energies). In the iron case the rate of the reaction (4) determines the overall reaction rate.

First let us discuss stable intermediates of the reaction. The N_2O molecular adsorption on the Fe site is notably weaker than on Co and Rh, hence N_2O is activated to a lesser extent on the former site. This correlates with the finding that the first N_2O decomposition step (2) has higher activation energy for Fe than for the other two metals, see table 1.

Table 1
Calculation results for $M(OH)_3(H_2O)_2$ cluster models. Distances are in Å, energies in kJ/mol.

Parameter	Fe	Co	Rh
Total spin	5/2	0	0
X cluster			
$R(M\text{–}OH_{planar})$	1.88	1.90	2.08
$R(M\text{–}OH_{axial})$	1.93	1.84	2.00
$R(M\text{–}OH_2)$	2.23	1.92	2.08
X·N₂O cluster			
$\Delta E_{ads}(N_2O)$	−16	−34	−44
$R(M\text{–}ON_2)$	2.62	2.16	2.31
Transition state 1			
Barrier height	41	28	35
$R(M\text{–}ON_2)$ in TS_1	2.14	1.89	2.06
$R(O\text{–}N_2)$ in TS_1	1.34	1.53	1.52
XO cluster			
$\Delta E(X + N_2O \rightarrow XO + N_2)$	−113	−76	−78
$R(M\text{–}O_{ads})$	1.80	1.73	1.88
XO·N₂O cluster			
$\Delta E_{ads}(N_2O)$	−28	−24	−26
$R(MO\text{–}ON_2)$	2.69	3.03	2.97
Transition state 2			
Barrier height	135	87	82
$R(M\text{–}OON_2)$ in TS_2	1.84	1.77	1.90
$R(MO\text{–}ON_2)$ in TS_2	1.81	1.93	1.95
$R(O\text{–}N_2)$ in TS_2	1.58	1.55	1.55
XO₂ cluster			
$\Delta E(XO + N_2O \rightarrow XO_2 + N_2)$	−132	−121	−122
$R(M\text{–}O_2)$	2.00	1.88	2.05
$R(O\text{–}O)$	1.41	1.39	1.39
$\Delta E(X\text{–}O_2 \rightarrow X + O_2)$	117	69	71

It is interesting to take a closer look at the electronic structure of the $OFe(OH)_3(H_2O)_2$ cluster as a model for the so-called α-oxygen formed after low-temperature N_2O decomposition on Fe/ZSM-5 [7] and compare it with the corresponding Al-containing model. The calculated Mulliken charge and spin density on the adsorbed oxygen atom, -0.43 and 1.07 a.u., respectively, suggest that it is essentially an O^- ion. These values change only slightly (to -0.48 and 0.90 a.u., respectively) when the calculation is repeated with the total spin equal to 3/2 instead of 5/2. The metal–oxygen bond energies in the XO clusters also differ between Fe and the other two metals. The $Fe\text{–}O_{ads}$ bond is stronger by about 35 kJ/mol than $Co\text{–}O_{ads}$ and $Rh\text{–}O_{ads}$ and by about 180 kJ/mol than $Al\text{–}O_{ads}$.

Some data on the computed transition states for the case of N_2O decomposition on Fe^{3+} are presented in table 2. The electronic structure of N_2O moiety in the transition state strongly resembles that of an N_2O^- ion. This suggests that N–O bond cleavage is achieved by electron donation from the metal to N_2O. From this observation one can conclude that electron-donor ligands coordinated to the metal should facilitate the N_2O dissociation. Indeed, our calculations of the reaction catalysed by the $Fe(OH)_3$ site, which differs from other models presented here by the absence of two wa-

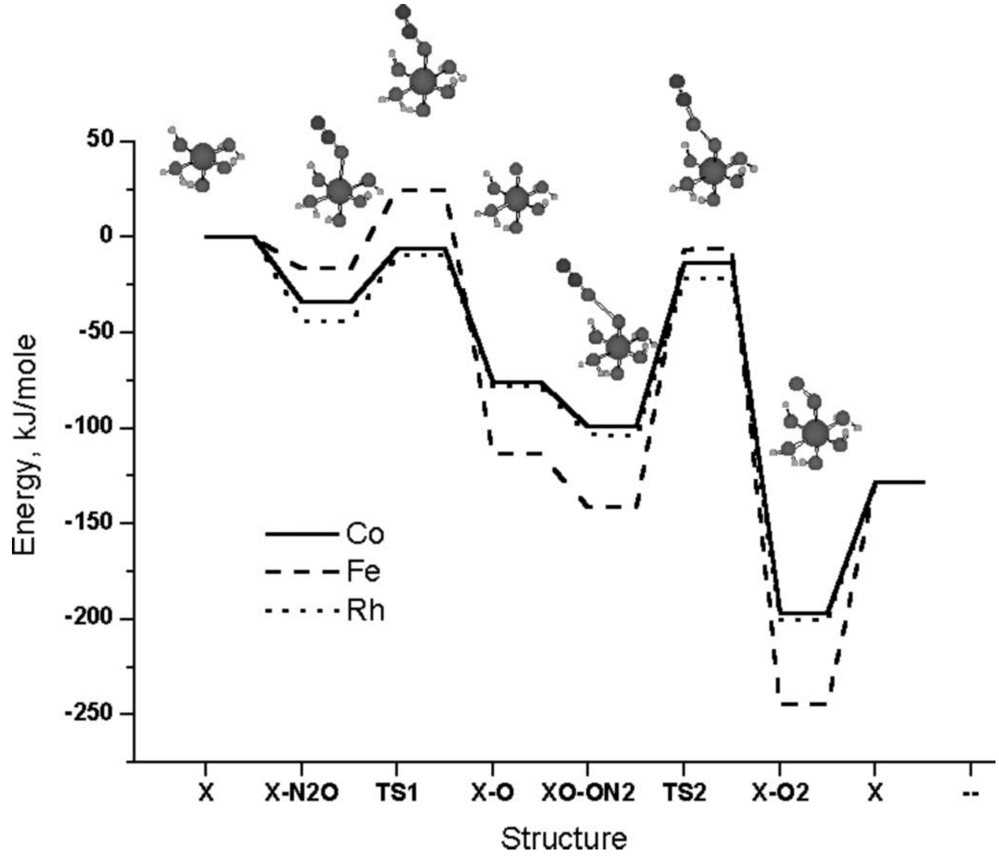

Figure 2. Energy diagrams of N_2O decomposition on Co (—), Fe (- - -) and Rh (· · ·) active sites. Corresponding cluster models are also shown.

Table 2

First and second transition states of N_2O dissociation on Fe site in comparison with N_2O^- and N_2O. Mulliken charges and atomic spin densities, as well as geometry parameters of the N_2O moiety are shown.

Atom	N_2O^-		TS_1 Fe–O–N_2		TS_2 FeO–O–N_2		N_2O
	Charge	Spin	Charge	Spin	Charge	Spin	charge
N(end)	−0.34	0.48	−0.08	0.38	0.02	0.03	−0.03
N(middle)	−0.05	0.23	0.17	0.09	0.22	0.12	0.39
O	−0.61	0.29	−0.44	0.01	−0.30	0.26	−0.36
			Geometry parameters in angstroms and degrees				
∠(N–N–O)	131.6		145.4		180		180
R(NO)	1.45		1.34		1.58		1.25
R(NN)	1.22		1.18		1.14		1.15

ter ligands, showed the increase in the activation energy by 40 kJ/mol. The calculated activation energy for the reaction (2) on a Fe site, 41 kJ/mol, agrees very well with experimental values 40–45 kJ/mol reported in [8]. The experimental values correspond to the low-temperature oxidation of Fe/ZSM-5 by N_2O.

The activation barrier for decomposition of the second N_2O molecule (reaction (4)) is much higher, 135 kJ/mol for Fe, 87 kJ/mol for Co and 82 kJ/mol for Rh (table 1, under *Transition state 2*). Obviously, the N_2O moiety in the second transition state does not have the features of an N_2O^- ion: it is linear, the major fraction of spin density is on the oxygen atom, and the N–O bond is much longer, 1.58 Å (table 2). Thus, one can conclude that the decomposition of the second N_2O molecule occurs through simultaneous dissociation of an N–O and formation of an O–O bond without an electron transfer. A weaker metal–oxygen bond should, in principle, facilitate this reaction. Indeed, as mentioned above, the absolute value of the total ΔE of the reactions (1) and (2) (see table 1, under *XO cluster*) is directly related to the metal–oxygen bond strength and is higher by *ca.* 35 kJ/mol for Fe than for Co and Rh. This correlates with the fact that the second activation energy is higher by *ca.* 50 kJ/mol in the former case. Noteworthy, unlike the X clusters, N_2O adsorption energies on the XO clusters are close for all the studied metals (table 1, under *XO·N_2O cluster*).

Experimental data reported in [1] show that the observed activation energies are 125–165 kJ/mol for Fe and 90–110 kJ/mol for Co-based catalysts. Thus, calculated activation energies for the step (4) lie within the corresponding intervals for experimental activation energies. The energy of the oxygen desorption is also higher for Fe (117 kJ/mol) than for Co and Rh (*ca*. 70 kJ/mol). Surprisingly, these energies are lower than the barriers of the reaction (4) for the corresponding sites by an almost constant amount about 12–18 kJ/mol. There is evidently a correlation between oxygen desorption energy and the M–O_{ads} bond strength. An analysis of the electronic structure of X–O_2 clusters shows that the adsorbed oxygen molecule has an O_2^- character: the Mulliken charge and total spin density of the O_2 moiety in $O_2Fe(OH)_3(H_2O)_2$ is equal to -0.49 and 1.01 a.u., respectively (compare with corresponding values for $OFe(OH)_3(H_2O)_2$ above). Thus, because both atomic and molecular oxygen adsorption involve metal oxidation from valence III to IV, there is a correlation between M–O_{ads} and M–O_2 bond energies.

4. Conclusions

We calculated the reaction energy diagrams of N_2O decomposition catalysed by single sites, including energies of intermediates and activation barriers. An analysis of the nature of the metal–oxygen bonds in adsorption complexes and the electronic structure of the transition states was attempted. The cluster model is represented by the formula $M(OH)_3(H_2O)_2$, where $M = $ Fe, Co, Rh. The results show that Co and Rh sites are more active than Fe. The rate-limiting step of the reaction is the formation of the adsorbed oxygen molecule via interaction of the adsorbed oxygen atom with N_2O. In this step a correlation between the strength of the metal–oxygen bond and the activation energy was found. A weaker metal-adsorbed oxygen bond for Co and Rh sites facilitates decomposition of the second N_2O molecule to form O_2, thus lowering the activation barrier. The analysis of the transition state of N_2O decomposition on $Fe(OH)_3(H_2O)_2$ indicates that N_2O dissociation is achieved by the electron density donation from the metal to an N_2O molecule.

Acknowledgement

Financial support from the Dutch Government (VROM/NOVEM), DSM AGRO and Hydro AGRI is gratefully acknowledged.

References

[1] F. Kapteijn, J. Rodrigues-Mirasol and J.A. Moulijn, Appl. Catal. B 9 (1996) 25.

[2] J. Leglise, J.O. Petunchi and W.K. Hall, J. Catal. 86 (1984) 392.

[3] H. Uetsuka, K. Aoyagi, S. Tanaka, K. Yuzaki, S. Ito, S. Kameoka and K. Kunimori, Catal. Lett. 66 (2000) 87.

[4] A. Yakovlev and G. Zhidomirov, Catal. Lett. 63 (1999) 91.

[5] B. te Velde and E.J. Baerends, J. Comp. Phys. 99 (1992) 84.

[6] K. Burke, J.P. Perdew and Y. Wang, in: *Electronic Density Functional Theory: Recent Progress and New Directions*, eds. J.F. Dobson, G. Vignale and M.P. Das (Plenum, New York, 1998).

[7] G.I. Panov, A.K. Uriarte, M.A. Rodkin and V.I. Sobolev, Catal. Today 41 (1998) 365.

[8] G.I. Panov, V.I. Sobolev and A.S. Kharitonov, J. Mol. Catal. 61 (1990) 85.